Clinical Radiology 74 (2019) 268–277

Contents lists available at ScienceDirect

Clinical Radiology

journal homepage: www.clinicalradiologyonline.net

Clinical utility of quantitative dual-energy CT iodine maps and CT morphological features in distinguishing small-cell from non-small-cell lung cancer

X. Xu [a], X. Sui [a], W. Zhong [b], Y. Xu [b], Z. Wang [c], J. Jiang [c], Y. Ge [d], L. Song [a], Q. Du [a], X. Wang [a], W. Song [a,*], Z. Jin [a,*]

[a] *Department of Radiology, Peking Union Medical College Hospital, Chinese Academy of Medical Sciences, Beijing, China*

[b] *Department of Respiratory Disease, Peking Union Medical College Hospital, Chinese Academy of Medical Sciences, Beijing, China*

[c] *Department of Epidemiology and Biostatistics, Institute of Basic Medical Science, Chinese Academy of Medical Sciences & School of Basic Medicine, Peking Union Medical College, Beijing, China*

[d] *Siemens China, Beijing, China*

ARTICLE INFORMATION

Article history:
Received 27 February 2018
Accepted 25 October 2018

AIM: To evaluate the clinical usefulness of quantitative dual-energy (DE) computed tomography (CT) iodine enhancement metrics combined with morphological CT features in distinguishing small-cell lung cancer (SCLC) from non-small-cell lung cancer (NSCLC).

MATERIALS AND METHODS: One hundred and six untreated lung cancer patients who underwent DECT before biopsy or surgery were prospectively enrolled. Twenty-seven routine CT descriptors, including tumour location, size, shape, margin, enhancement heterogeneity, and internal and surrounding structures, and associated findings were assessed and DECT parameters were measured in all patients. Multiple logistic regression analyses were applied to identify independent predictors of SCLC. The area under the receiver operating characteristic curve was compared between CT features combined with DECT metrics and CT features alone for distinguishing SCLC from NSCLC.

RESULTS: Histology revealed NSCLC in 80 and SCLC in 26 patients. In univariate analysis, 12 morphological CT features and two DECT metrics differed significantly between NSCLC and SCLC. When DECT parameters were combined with CT features for multivariate analysis, the independent predictors of SCLC were large tumour size, central location, confluent mediastinal lymphadenopathy, homogeneous enhancement, absence of coarse spiculation, and lower iodine density and iodine ratio (all $p<0.05$). The area under the receiver operating characteristic curve was improved from 0.908 to 0.981 after adding DECT metrics compared with CT features alone ($p=0.007$).

* Guarantor and correspondent: Z. Jin, Peking Union Medical College Hospital (East), No.1 Shuaifuyuan Wangfujing Dongcheng District, Beijing, 100730, China. Tel.: +13601037675; fax: +861069155442. W. Song, Peking Union Medical College Hospital (East, No.1 Shuaifuyuan Wangfujing Dongcheng District, Beijing, 100730, China. Tel.: +8613601069220; fax: +861069155442.

E-mail addresses: cjr.songwei@vip.163.com (W. Song), jin_zhengyu@163.com (Z. Jin).

https://doi.org/10.1016/j.crad.2018.10.012

CONCLUSION: The combination of DECT measures and CT morphological features can be used to distinguish SCLC from NSCLC, with higher diagnostic performance compared with CT morphological features alone.

Introduction

Lung cancer is one of the most common malignancies worldwide and remains the leading cause of cancer-related death in both men and women.[1,2] Small-cell lung cancer (SCLC) tends to behave differently from non-small-cell lung cancer (NSCLC) in clinical properties, with characteristics of rapid tumour growth, early development of widespread metastases, responsiveness to specific chemoradiotherapy, and poor prognosis. Hence, it is critical for clinicians to confirm the diagnosis of SCLC or NSCLC to achieve early and accurate therapeutic planning as well as prognostication. Imaging techniques can provide qualitative or quantitative information for tumour detection, characterisation, staging, and evaluation of therapeutic response in clinical practice, displaying potential complementary value for differentiation of lung cancer subtypes.[3] In clinical routine, contrast-enhanced computed tomography (CT) is typically the first investigation for patients with suspected lung malignancy. Evaluation of lesions with conventional CT is based on two major criteria: morphological features (such as size, margins, density, and internal and surrounding characteristics) and degree of enhancement.[4] CT features provide qualitative morphological information and play an indispensable role in imaging diagnosis. Many previous studies have described CT morphological features of lung cancer subtypes,[5,6] such as SCLC more commonly manifests as a hilar mass with confluent mediastinal lymphadenopathy and adenocarcinoma more commonly shows as a spiculate mass with air bronchogram or bubble-like lucency, but few studies have reported the diagnostic accuracy of imaging features in distinguishing SCLC from NSCLC.

The degree of enhancement of lung lesions can be determined in routine single-energy enhanced CT, but the measurement error caused by misregistration of the region of interest between pre- and post-contrast images is unavoidable.[7] Dual-energy CT (DECT) is a promising imaging technique that can be used for analysis of CT morphological features, as well as quantification of iodine concentration and enhancement in tumours.[3,8] With one single contrast-enhanced scan, DECT offers two CT series of virtual non-contrast and iodine-enhanced images, omitting the need for non-enhanced CT and eliminating the measurement error caused by two separate CT examinations. As a result of the energy dependence of the attenuation coefficient of different materials, DECT makes it possible to optimise the differentiation of lung nodules or masses.[8] Several studies have reported the positive correlation between DECT parameters and the expression level of vascular endothelial growth factor and hypoxia-inducible factor-1 in patients with NSCLC,[9,10] indicating that DECT could be a valuable method for imaging tumour angiogenesis. Additionally, different patterns of the microvascular network have been observed in various histological types of lung cancer in previous studies.[11,12] Thus, it is postulated that quantitative DECT parameters might be different between SCLC and NSCLC, and DECT metrics combined with CT features may further promote the differential accuracy compared with CT features alone. To the authors' knowledge, no previous studies have investigated the diagnostic performance of iodine parameters and morphological features in distinguishing lung cancer subtypes.

Therefore, the aim of this study was to evaluate prospectively the clinical usefulness of quantitative DECT iodine enhancement metrics combined with morphological CT features in distinguishing SCLC from NSCLC.

Materials and methods

Study population

This single-centre prospective study was approved by the Medical Ethics Committee of Peking Union Medical College Hospital, and written informed consent was obtained from all patients. Between December 2015 and October 2016, 146 consecutive patients with clinically or radiologically suspected lung cancer underwent DECT. Patients were finally enrolled if they fulfilled the following criteria: solid tumour with a minimum transverse diameter of 10 mm; no previous treatment for lung cancer or other malignancies; and histologically confirmed lung cancer subtype. The histological diagnosis was based on the World Health Organization classification published in 2015.[13] Pregnant women and patients who had a history of contrast material reaction and impaired renal function (creatinine $>$1.5 mg/dl and/or glomerular filtration rate $<$60 ml/min) were excluded. Finally, 106 patients (median age, 62 years; range, 35–81 years) comprised the study population (Electronic Supplementary Material Figure S1).

DECT protocol

All CT examinations were performed on a third-generation dual-source CT unit (SOMATOM Force; Siemens Healthcare, Forchheim, Germany). Contrast material (30 ml iopromide, Ultravist 370; Bayer Schering Pharma, Berlin, Germany) was administered via an antecubital vein at an intended flow rate of 3 ml/s, followed by 30 ml of

saline, injected at the same flow rate. After the injection, scans were started using a bolus-tracking technique with a threshold of 70 HU in the descending aorta and an additional delay of 6 seconds.[14] A combination of tin-filtered 150 and 90 kV was used for dual-energy scanning. The quality reference tube current of tubes A and B was set to 46 and 60 mAs, respectively. Automatic tube current modulation (CARE Dose 4D) was used. By combining the tin-filtered 150 and 90 kV data with a weighting factor of 0.6,[15] another series of weighted-average datasets equivalent to 120 kV images was automatically generated. Collimation was set to 192×0.6 mm. Pitch was 1.0 at a rotation time of 0.25 s/rotation. Datasets of tin-filtered 150, 90, and virtual 120 kV were reconstructed with advanced modelled iterative reconstruction (ADMIRE) using a soft-tissue kernel (Qr36) at a section thickness of 1.5 mm with a 1.2 mm increment. All CT data acquisition was performed in a caudocranial direction during a deep-inspiratory breath hold from the lung bases up to the apices.

Mean volume CT dose index and dose–length product for DECT acquisition were 2.78±0.75 mGy and 108.41±30.50 mGy·cm, respectively, corresponding to an effective radiation dose of 1.52±0.43 mSv (using a standard conversion factor for chest CT of 0.014 mSv/mGy·cm).[16] The mean body mass index of patients was 23.59±3.33 (range 18.08–31.25).

Analysis of CT morphological features

Virtual 120 kV images were applied to evaluate morphological CT features and viewed at mediastinal (width, 400 HU; level, 40 HU) and lung (width, 1500 HU; level, −400 HU) window settings for axial images on a picture archiving and communications system. Two radiologists (with 25 and 5 years of experience in thoracic radiology, respectively) interpreted all of the CT images in a consensual manner.[5] The radiologists were blinded to clinical and pathological data. CT morphological features analysed for each lesion included tumour location, size (maximum long-axis diameter), shape, margin, enhancement heterogeneity, and internal and surrounding structures, and associated findings. Analysis was based on previously published evaluation methods,[6,17] among which, coarse spiculation was defined as linear strands ≥2 mm thick, and fine spiculation was defined as linear strands <2 mm. Homogeneous enhancement was defined as visually >90% of the area with the same attenuation value. In total, 27 descriptors of tumours on DECT images were reviewed (Electronic Supplementary Material Table S1).

Quantitative analysis of DECT data

All measurements were performed in consensus by two experienced radiologists (with 5 and 8 years of experience in thoracic imaging, respectively) who were unaware of the clinical and pathological results. Datasets of tin-filtered 150 and 90 kV were transferred to a commercially available DE-equipped workstation (Syngo.via VB10, Dual Energy, Siemens, Healthineers, Forchheim, Germany) and analysed by the virtual non-contrast application mode. The region of interest was drawn freehand around the tumour in the axial section. It was maximised by including as much as possible of the mass and excluding any area of obviously gross necrosis, calcification and large vessels (mean size of regions of interest, 9.71±8.54 cm^2). The iodine density (in mg/ml) of each lung lesion was noted. The radiologists placed the region of interest in the artery and main tumour of concern successively to calculate iodine ratio (%). The latter was defined as the ratio of iodine density of the lung lesion to that of the descending aorta or subclavian artery on the same section, to minimise variations caused by circulation status and scan times. Three measurements were conducted, and average values were recorded.

Statistical analysis

All statistical analyses were performed using commercially available software (SPSS version 20.0; SPSS, Chicago, IL, USA). Continuous variables were presented as mean ± standard deviation. Differences in CT features and DECT metrics between NSCLC and SCLC were compared using the χ^2 test for categorical data and Student's *t*-test (normal distribution) or Mann–Whitney *U* test (non-normal distribution) for continuous variables. Box and whisker plots were generated to visualise group differences for the distributions of quantitative DECT metrics. Multivariate logistic regression analyses were applied to identify independent predictors of SCLC or NSCLC, with the model of CT features alone and CT features combined with DECT metrics. Factors with $p<0.05$ on univariate analysis were used as the input variables for multiple logistic regression analysis, with the final model selected with the backward elimination method.[18] Comparison between two areas under the receiver operating characteristic curve was made to identify the ability of the two models to discriminate SCLC

Table 1
Clinical characteristics of lung cancer patients.

Variable	NSCLC	SCLC	*p*-Value
No. of patients	80	26	
Median age (year)[a]	62 (35–81)	61 (38–79)	0.496
Women	60.5 (41–81)	61.5 (48–70)	0.560
Men	64.5 (35–79)	61 (38–79)	0.250
Sex			0.619
Female	24 (30%)	6 (23.1%)	
Male	56 (70%)	20 (76.9%)	
TNM stage			**0.008**
I	9	0	
II	12	0	
III	33	19	
IV	26	7	
Diagnostic technique			
Fine-needle aspiration biopsy	1	1	**0.008**
Core-needle biopsy	36	10	
Surgery	23	1	
Transbronchial biopsy	20	14	

Unless otherwise indicated, data are number of patients. Values in bold indicate statistical significance, $p<0.05$.
NSCLC, non-small-cell lung cancer; SCLC, small-cell lung cancer; TNM, tumour–node–metastasis.
[a] Data in parentheses indicates the range.

Table 2
Association between CT characteristics with lung cancer subtypes.

Characteristics	NSCLC	SCLC	*p*-Value	Univariate OR (95% CI)
Location				
Distribution			**0.012**	
Central	42	21		3.800 (1.304–11.073)
Peripheral	38	5		Reference
Lobe location			0.640	
Right upper lobe	20	4		Reference
Right middle lobe	8	1		0.594 (0.057–6.175)
Right lower lobe	13	5		1.827 (0.411–8.123)
Left upper lobe	21	6		1.357 (0.332–5.554)
Left lower lobe	18	10		2.639 (0.700–9.945)
Long-axis diameter (cm) [a]	4.9±2.1 (1.76–10.59)	6.2±2.7 (2.43–12.4)	**0.014**	NA
Shape				
Contour			0.897	
Round	0	0		Reference
Somewhat irregular	35	11		Reference
Irregular	45	15		1.061 (0.434–2.595)
Lobulation			0.931	
None	5	1		Reference
Lobulation number less than 3	20	6		1.500 (0.146–15.461)
Lobulation number between 4 and 6	44	16		1.818 (0.197–16.774)
Lobulation number more than 6	11	3		1.364 (0.112–16.577)
Margin				
Border definition			0.758	
Well defined	8	2		Reference
Between well and poorly defined	53	16		1.208 (0.233–6.271)
Poorly defined	19	8		1.684 (0.291–9.750)
Spiculation			**0.005**	
None	12	12		Reference
Fine spiculation	52	13		0.250 (0.092–0.683)
Coarse spiculation	16	1		0.063 (0.007–0.549)
Internal				
Air bronchogram			0.549	
No	63	19		Reference
Yes	17	7		1.365 (0.493–3.782)
Air Space			0.633	
No	61	21		Reference
Yes	19	5		0.764 (0.254–2.303)
Enhancement heterogeneity			**0.044**	
Homogeneous	15	10		6.222 (1.482–26.119)
Slight or moderate heterogeneous	37	13		3.279 (0.852–12.624)
Marked heterogeneous	28	3		Reference
Surrounding structure				
Marginal ground-glass opacity			0.733	
No	40	14		Reference
Yes	40	12		0.857 (0.353–2.081)
Fissure attachment			0.930	
No	50	16		Reference
Yes	30	10		1.042 (0.419–2.589)
Pleural attachment			0.087	
No	43	19		Reference
Yes	37	7		0.428 (0.162–1.131)
Vascular convergence			**0.011**	
No	44	22		4.500 (1.421–14.252)
Yes	36	4		Reference
Thickened adjacent bronchovascular bundles			**0.017**	
No	46	22		4.065 (1.282–12.889)
Yes	34	4		Reference
Pleural retraction			**0.005**	
No	38	21		4.642 (1.593–13.526)
Yes	42	5		Reference
Peripheral emphysema			0.855	
Absence	47	14		Reference
Slight or moderate	26	10		1.291 (0.503–3.313)
Severe	7	2		0.959 (0.179–5.152)
Peripheral fibrosis			0.576	
Absence	54	18		Reference
Slight or moderate	21	5		0.714 (0.235–2.171)

(*continued on next page*)

Table 2 (*continued*)

Characteristics	NSCLC	SCLC	*p*-Value	Univariate OR (95% CI)
Severe	5	3		1.800 (0.391–8.292)
Associated findings				
Nodules in primary tumour lobe			0.779	
No	53	18		Reference
Yes	27	8		0.872 (0.336–2.263)
Nodules in non-tumour lobes			0.342	
No	57	21		Reference
Yes	23	5		0.590 (0.199–1.753)
Lymphadenopathy			**0.038**	
No	21	1		Reference
Yes	59	25		8.898 (1.134–69.808)
Confluent mediastinal lymphadenopathy			**0.000**	
No	73	11		Reference
Yes	7	15		14.221 (4.741–42.658)
Encasement of mediastinal structures			**0.004**	
No	64	13		Reference
Yes	16	13		4.000 (1.556–10.281)
Vascular involvement			**0.005**	
No	48	7		Reference
Yes	32	19		4.071 (1.535–10.796)
Lung atelectasis and/or obstructive pneumonia				
No	60	13	**0.019**	Reference
Yes	20	13		3 (1.195–7.531)
Pleural effusion of tumour side				
No	61	18	0.477	Reference
Yes	19	8		1.427 (0.536–3.799)
Pleural effusion of non-tumour side			0.420	
No	77	24		Reference
Yes	3	2		2.139 (0.337–13.561)

Unless otherwise indicated, data are number of patients. Values in bold indicate statistical significance, $p<0.05$.
CT, computed tomography; NSCLC, non-small-cell lung cancer; SCLC, small-cell lung cancer; OR, odds ratio; CI, confidence interval; NA: not applicable.
[a] Data are mean±standard deviation (the range); $p<0.05$.

from NSCLC. Differences were considered statistically significant at a two-tailed *p*-value <0.05.

Results

Patients

The clinical data are summarised in Table 1. Histology revealed adenocarcinoma in 44 patients, squamous cell carcinoma in 36 and SCLC in 26. Compared with NSCLC, tumour staging for SCLC was late, with all patients in stage III/IV ($p=0.008$).

CT characteristics of lung cancer subtypes

Univariate analysis revealed that 12 CT features differed significantly between NSCLC and SCLC (Table 2): tumour distribution, long-axis diameter, spiculation, enhancement heterogeneity, vascular convergence, thickened adjacent bronchovascular bundles, pleural retraction, lymphadenopathy, confluent mediastinal lymphadenopathy, encasement of mediastinal structures, vascular involvement, lung atelectasis, and/or obstructive pneumonia (all $p<0.05$). SCLC was more likely to be located within the central aspect of the chest (odds ratio [OR]: 3.8; 95% confidence interval [CI]: 1.304–11.073), while NSCLC was more frequently found in the periphery. Long-axis tumour diameter in SCLC was significantly larger than in NSCLC ($p=0.014$). Tumours with lymphadenopathy (OR: 8.898; 95% CI: 1.134–69.808), confluent mediastinal lymphadenopathy (OR: 14.221; 95% CI: 4.741–42.658), encasement of mediastinal structures (OR: 4; 95% CI: 1.556–10.281), homogeneous enhancement (OR: 6.222; 95% CI: 1.482–26.119), vascular involvement (OR: 4.071; 95% CI: 1.535–10.796), and lung atelectasis and/or obstructive pneumonia (OR: 3; 95% CI: 1.195–7.531) were more frequently found among SCLC (Fig 1). Tumours with spiculation (OR of fine spiculation: 0.250; 95% CI: 0.092–0.683; OR of coarse spiculation: 0.063; 95% CI: 0.007–0.549), vascular convergence (OR: 4.50; 95% CI: 1.421–14.252), thickened adjacent bronchovascular bundles (OR: 4.065, 95% CI: 1.282–12.889), and pleural retraction (OR: 4.642; 95% CI: 1.593–13.526) were more likely to be observed among NSCLC. When it came to other CT features, no significant differences were noted between NSCLC and SCLC.

Quantitative iodine analyses with DECT

Comparisons of DECT quantitative parameters between NSCLC and SCLC are displayed in box-plots (Fig 2). Iodine density (SCLC: 1.17±0.28 mg/ml versus NSCLC: 1.55±0.47 mg/ml; $p=0.001$) and iodine ratio (SCLC: 11.59±2.62% versus NSCLC: 16.27±6.18%; $p=0.000$) were significantly lower in SCLC compared with NSCLC (Figs 1 and 3).

Multivariable analysis and receiver operating characteristic curve analysis

In multivariate analysis, for the model with CT features alone, long-axis diameter, enhancement heterogeneity and

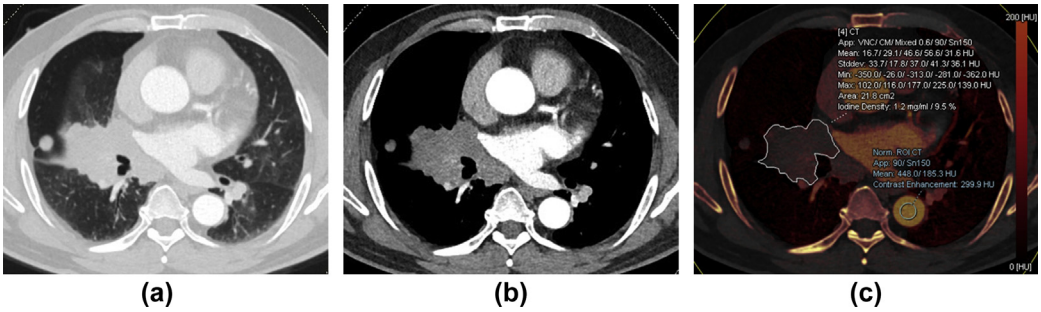

Figure 1 Representative dual-energy CT images of a 64-year-old man with SCLC. (a) Lung window of virtual 120-kV images shows a large mass in the right perihilar lung. (b) Mediastinal window shows confluent lymphadenopathy and homogeneous enhancement of the tumour. (c) Iodine density and iodine ratio of the iodine map with ROI drawn on the perihilar mass lesion was 1.2 mg/ml and 9.5%, respectively.

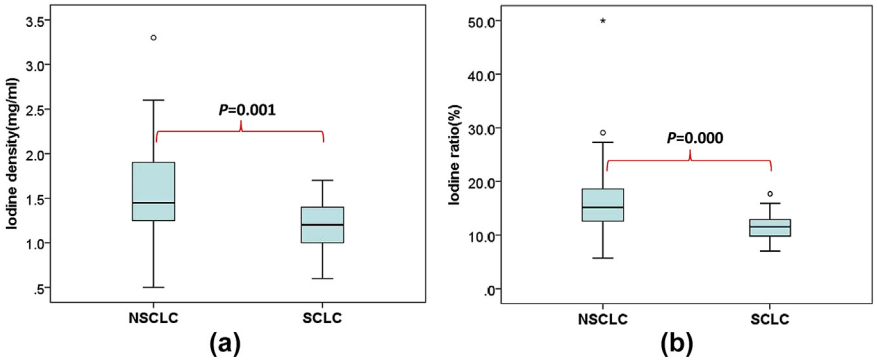

Figure 2 Boxplots presenting the distribution of iodine density (a) and iodine ratio (b) in patients with NSCLC and SCLC, respectively.

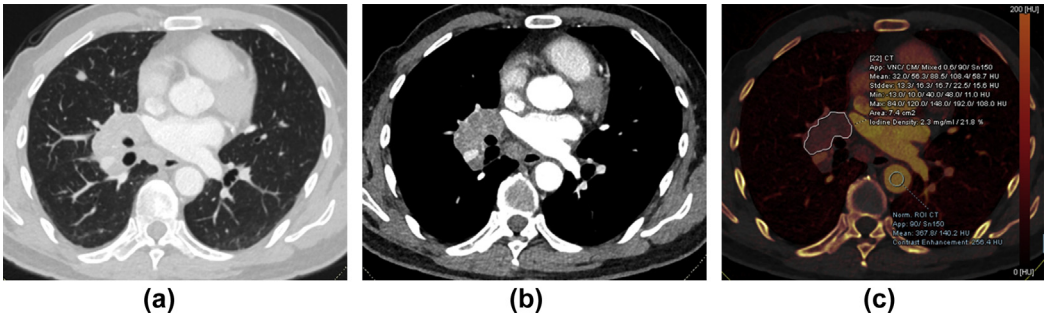

Figure 3 Axial contrast-enhanced dual-energy CT images of a 57-year-old man with adenocarcinoma. (a) Lung window of virtual 120 kV images shows a round-like well-defined mass located in the right perihilar lung, presenting no spiculation. (b) Mediastinal window shows homogeneous enhancement of the tumour and subcarinal lymphadenopathy. (c) Iodine density and iodine ratio of the iodine map with ROI drawn on the perihilar mass lesion was 2.3 mg/ml and 21.8%, respectively.

confluent mediastinal lymphadenopathy were proved to be independent prognostic factors of lung cancer subtypes when adjusting for spiculation and lymphadenopathy (Electronic Supplementary Material Table S2). When DECT metrics were added, lymphadenopathy was excluded from the model, while distribution, pleural retraction and lung atelectasis and/or obstructive pneumonia were included, regardless of statistical significance. Finally, the most important and significantly independent predictive factors for SCLC were large tumour size, central location, homogeneous enhancement, confluent mediastinal lymphadenopathy, absence of coarse spiculation, and lower iodine density and iodine ratio when adjusting for pleural retraction and lung atelectasis and/or obstructive pneumonia (Table 3). The area under the receiver operating characteristic curve increased markedly from 0.908 (95% CI: 0.852–0.963) to 0.981 (95% CI: 0.961–1.0) when DECT metrics were added (p=0.007; Fig 4), the diagnostic sensitivity grew from 80% to 91.3%, and specificity rose from 88.5% to 96.2%.

Discussion

We reported a significant difference in quantitative DECT parameters between SCLC and NSCLC in patients with solid tumours diameter >1 cm. The combination of CT morphological features with DECT metrics markedly improved the

Table 3
Multivariable regression analysis of DECT metrics combined with CT features predicting SCLC from NSCLC.

Variable and level	Odds ratio		*p*-Value
	Point estimate	95% CI	
Long-axis diameter (cm)	1.720	1.022–2.895	**0.041**
Distribution			
Central	33.731	1.495–761.071	**0.027**
Peripheral	Reference		
Spiculation			
None	546.343	1.663–179517.367	**0.033**
Fine spiculation	109.742	1.019–11818.289	**0.049**
Coarse spiculation	Reference		
Pleural retraction			
No	9.769	0.435–219.613	0.151
Yes	Reference		
Lung atelectasis and/or obstructive pneumonia			
No	Reference		
Yes	14.986	0.914–245.621	0.058
Enhancement heterogeneity			
Homogeneous	259.796	3.489–19343.101	**0.011**
Slight or moderate heterogeneous	0.198	0.006–6.494	0.363
Marked heterogeneous	Reference		
Confluent mediastinal lymphadenopathy			**0.001**
No	Reference		
Yes	697.023	13.710–35438.058	
Iodine ratio (%)	0.460	0.269–0.786	**0.005**
Iodine density (mg/ml)	0.002	0.000–0.207	**0.009**

Values in bold indicate statistical significance, $p<0.05$.
DECT, dual-energy computed tomography; NSCLC, non-small-cell lung cancer; SCLC, small-cell lung cancer; CI, confidence interval.

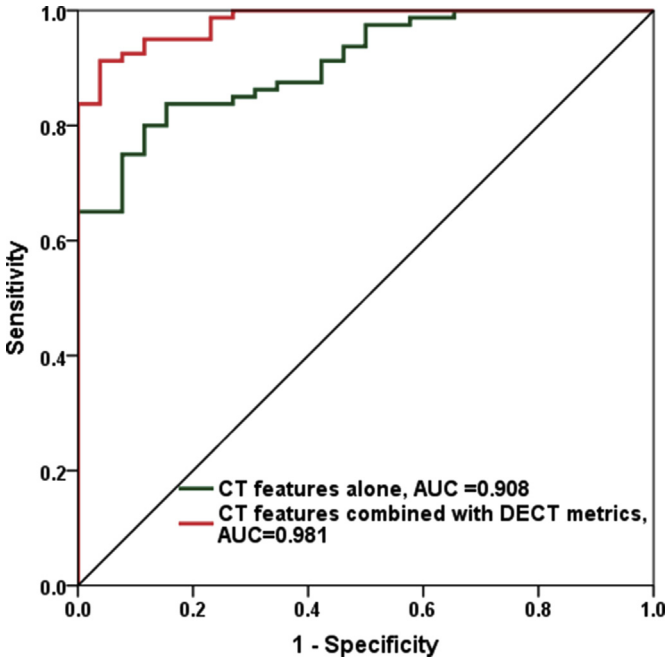

Figure 4 Receiver operating characteristic curves applied to predict small-cell lung cancer from non-small-cell lung cancer with CT features alone and combined with DECT metrics. AUC: Area under the ROC curve; 95% CI: confidence interval.

diagnostic ability, sensitivity and specificity in distinguishing SCLC from NSCLC compared with CT features alone, validating DECT as an effective imaging technique in diagnosing lung cancer subtypes. Consequently, DECT can non-invasively provide additional information for pre-treatment evaluation of lung cancer before it can be achieved by pathological determination.

Treatment and prognosis differ between SCLC and NSCLC. SCLC is frequently metastatic at initial diagnosis and mostly treated with chemoradiotherapy and rarely undergoes surgical resection (<5% of cases).[19] The median survival time of SCLC after diagnosis is only 2–4 months in the absence of treatment and 8–20 months in patients under treatment.[6,19] In contrast, NSCLC has demonstrated notable improvements in survival time owing to a high level of surgical opportunity and rapid development of individualised therapies based on specific histological and molecular subtypes.[20] Therefore, qualitative and quantitative metrics derived from DECT would be of value in assisting clinical estimation of tumour subtypes to contribute to initial treatment selection and prognostic prediction, especially when invasive procedures are unavailable or pathological results indeterminate.[21]

In pursuit of high contrast-to-noise ratio and fine image quality in evaluating anatomical structures in DECT, fused images, taking advantage of both low- and high-voltage images, are frequently applied to assess morphological features.[15] In the current study, 27 CT features were analysed on virtual 120 kV images and it revealed nine morphological features more likely to be indicative of SCLC rather than NSCLC, including central location, large size, absence of spiculation, lymphadenopathy, confluent mediastinal lymphadenopathy, encasement of mediastinal structures, vascular involvement, lung atelectasis and/or obstructive pneumonia, and homogeneous enhancement. Kazawa *et al.*[22] demonstrated that a central mass accompanied with mediastinal extension was the most common feature in

SCLC, and great vessel wall involvement was frequently observed at advanced stages. Lee *et al.*[23] reported that characteristic CT features of SCLC were confluent mediastinal lymphadenopathy, with less manifestation of spiculation. In addition, Carter *et al.*[6] concluded that encasement of mediastinal structures was mostly present in SCLC. These findings are consistent with the present results, in spite of the fact that statistical comparison was not performed between SCLC and NSCLC in the previous studies. Furthermore, the contrast enhancement pattern of lung cancer subtypes was not analysed in the previous studies, while we made a detailed analysis and revealed a significant difference between SCLC and NSCLC. In multivariate analysis, the c-statistic of morphological features in diagnosing SCLC was 0.908, validating the diagnostic value of morphological features in discrimination of SCLC and NSCLC.

DECT images revealed CT morphological features of the tumours and provided quantitative data of iodine maps for clinical diagnosis, offering added objective information for tissue characterisation. In recent years, DECT has proved useful in evaluating neoangiogenesis and applied increasingly in tumour detection and characterisation.[24] Previous studies have revealed that net iodine value can be objectively and quantitatively measured in DECT and reflects the level of underlying tumour angiogenesis.[18,24] In the current study, iodine density and iodine ratio were markedly lower in SCLC compared with NSCLC. This discrepancy might be explained by the distinct difference in the vascularity and vasculature between SCLC and NSCLC. Compared with SCLC, the vascular bed of adenocarcinoma and squamous cell carcinoma comprises many large vessels, which allows greater tumour blood volume,[11,12] resulting in higher iodine-related metrics. Besides, tumour necrosis was more common and extensive in SCLC compared with NSCLC,[21] which further explained the lower iodine-enhanced parameters in SCLC. This finding in the present study was consistent with the results of dynamic volume perfusion CT conducted by Shi *et al.*[25] They showed that dynamic volume perfusion CT parameters of adenocarcinoma and squamous cell carcinoma, including blood volume, blood flow and permeability, were significantly higher compared with those of SCLC. Similarly, Spira *et al.*[26] correlated volume perfusion CT with histopathological results in assessing lung cancer vascularity, and confirmed that the parameter transit constant representing capillary permeability was reduced in SCLC as compared with adenocarcinoma. Good correlation between iodine enhancement metrics from DECT and perfusion parameters from dynamic volume perfusion CT has been validated by studies performed in lung and liver,[27,28] which may explain the consistency between previous dynamic volume perfusion CT findings and the present results.

When combining DECT metrics with CT morphological features for multivariate analysis, the diagnostic power was significantly improved compared with CT features alone, thus verifying the added diagnostic value of DECT parameters. In this study, the discrepancy arising from different positions of regions of interest in routine contrast-enhanced CT was avoided when assessing the degree of enhancement of tumours. Furthermore, radiation dose was significantly decreased because the unenhanced CT scan was not required. With the advancement of scanning techniques and image reconstruction software, DECT renders further reduction of acquisition time and radiation dose, which would be especially beneficial to patients undergoing tumour evaluation and therapeutic monitoring.[29]

In this investigation, both morphological and quantitative parameters were evaluated. Although quantitative data are increasingly being studied, CT morphological features of lung cancer are still indispensable contributors to oncological practice owing to their ready accessibility. In the era of precision medicine and big data, single risk factors are considered unreliable and estimation based on a multivariable model is now required. Radiomics, which is based on this principle, uses data mining from images to acquire high-throughput of quantitative imaging features and forms a radiomic signature for clinical use.[30] Other studies have confirmed the incremental value of radiomic signatures derived from conventional CT in the diagnosis and prognosis of lung cancer, making precision medical treatment more achievable.[30,31] The current study revealed the superiority of DECT over conventional contrast-enhanced CT in the differential diagnosis of lung cancer subtypes. This indicates that DECT images may provide more valuable imaging markers in constructing radiomic signatures and render more possibilities for the application of radiomics in the future.

There were some limitations to this study. First, the sample size of the SCLC group was small owing to the lower incidence of SCLC compared with NSCLC.[19] Second, SCLC stages I and II were not analysed and only the three most common histological subtypes of lung cancer were studied, thus investigations related to early-stage SCLC and uncommon lung cancer subtypes are necessary in the future. Third, tumours with a diameter <1 cm were excluded from the study group considering that the measurements were susceptible to the effect of volume averaging, thus selection bias maybe present. Finally, considering the spatial heterogeneity regarding vascularity in lung cancer, a potential bias was that manual regions of interest may not be representative of total tumour vascularity; however, the method of manual regions of interest placed in a maximum slice of tumour area in this study has been verified as an efficient and reliable measurement, which has been widely applied in previous studies.[18,27,32] In the present study, the correlation of iodine-enhanced parameters with morphology of the microvascular bed in lung cancer lesions was not investigated, it requires one-to-one match analysis between pathological morphology and DECT measurements, and would be further conducted in subsequent research.

In conclusion, the combination of DECT metrics and morphological CT features facilitates the discrimination of SCLC and NSCLC appearing as solid lesions, leading to more accurate diagnosis than using CT features alone. In the clinical setting, these findings would be useful for interpretation of DECT features and may help physicians with preliminary planning of lung cancer management and prognostic prediction.

Conflict of interest

There are no actual or potential conflicts or interest to declare in relation to this article.

Acknowledgements

The authors thank Cathel Kerr, PhD, from Liwen Bianji, Edanz Editing China (www.liwenbianji.cn/ac), for editing the English text of a draft of this manuscript. This project was funded by the Health Industry Special Scientific Research Project (201402019) and the National Public Welfare Basic Scientific Research Project (2017PT32004). The funding source had no involvement in the conduct of the research and/or preparation of the article.

Appendix A. Supplementary data

Supplementary data to this article can be found online at https://doi.org/10.1016/j.crad.2018.10.012.

References

1. Byers T, Wender RC, Jemal A, *et al*. The American Cancer Society challenge goal to reduce US cancer mortality by 50% between 1990 and 2015: results and reflections. *CA Cancer J Clin* 2016;**66**(5):359–69 https://doi:10.3322/caac.21348.
2. Chen W, Zheng R, Baade PD, *et al*. Cancer statistics in China, 2015. *CA Cancer J Clin* 2016;**66**(2):115–32 https://doi:10.3322/caac.21338.
3. Tabari A, Lo Gullo R, Murugan V, *et al*. Recent advances in computed tomographic technology: cardiopulmonary imaging applications. *J Thorac Imaging* 2017;**32**(2):89–100 https://doi:10.1097/rti.0000000000000258.
4. Zhang Y, Cheng J, Hua X, *et al*. Can spectral CT imaging improve the differentiation between malignant and benign solitary pulmonary nodules? *PLoS One* 2016;**11**(2):e0147537 https://doi:10.1371/journal.pone.0147537.
5. Nakazono T, Sakao Y, Yamaguchi K, *et al*. Subtypes of peripheral adenocarcinoma of the lung: differentiation by thin-section CT. *Eur Radiol* 2005;**15**(8):1563–8 https://doi:10.1007/s00330-004-2595-7.
6. Carter BW, Glisson BS, Truong MT, *et al*. Small cell lung carcinoma: staging, imaging, and treatment considerations. *RadioGraphics* 2014;**34**(6):1707–21 https://doi:10.1148/rg.346140178.
7. Ko JP. Lung nodule detection and characterization with multi-slice CT. *J Thorac Imaging* 2005;**20**(3):196–209.
8. Chae EJ, Song JW, Krauss B, *et al*. Dual-energy computed tomography characterization of solitary pulmonary nodules. *J Thorac Imaging* 2010;**25**(4):301–10 https://doi:10.1097/RTI.0b013e3181e16232.
9. Li GJ, Gao J, Wang GL, *et al*. Correlation between vascular endothelial growth factor and quantitative dual-energy spectral CT in non-small-cell lung cancer. *Clin Radiol* 2016;**71**(4):363–8 https://doi:10.1016/j.crad.2015.12.013.
10. Yanagawa M, Morii E, Hata A, *et al*. Dual-energy dynamic CT of lung adenocarcinoma: correlation of iodine uptake with tumour gene expression. *Eur J Radiol* 2016;**85**(8):1407–13 https://doi:10.1016/j.ejrad.2016.05.016.
11. Zielinski KW, Kulig A, Zielinski J. Morphology of the microvascular bed in primary human carcinomas of lung. Part II. Morphometric investigations of microvascular bed of lung tumours. *Pathol Res Pract* 1984;**178**(4):369–77 https://doi:10.1016/s0344-0338 (84)80029-1.
12. Zielinski KW, Kulig A. Morphology of the microvascular bed in primary human carcinomas of lung. Part I: three-dimensional pattern of microvascular network. *Pathol Res Pract* 1984;**178**(3):243–50 https://doi:10.1016/s0344-0338 (84)80106-5.
13. Marx A, Chan JK, Coindre JM, *et al*. The 2015 World Health Organization classification of tumours of the thymus: continuity and changes. *J Thorac Oncol* 2015;**10**(10):1383–95 https://doi:10.1097/jto.0000000000000654.
14. Li X, Meng X, Ye Z. Iodine quantification to characterize primary lesions, metastatic and non-metastatic lymph nodes in lung cancers by dual energy computed tomography: an initial experience. *Eur J Radiol* 2016;**85**(6):1219–23 https://doi:10.1016/j.ejrad.2016.03.030.
15. Paul J, Bauer RW, Maentele W, *et al*. Image fusion in dual energy computed tomography for detection of various anatomic structures—effect on contrast enhancement, contrast-to-noise ratio, signal-to-noise ratio and image quality. *Eur J Radiol* 2011;**80**(2):612–9 https://doi:10.1016/j.ejrad.2011.02.023.
16. Task Group on Control of Radiation Dose in Computed Tomography. Managing patient dose in computed tomography. A report of the International Commission on Radiological Protection. *Ann ICRP* 2000;**30**(4):7–45.
17. Liu Y, Kim J, Qu F, *et al*. CT Features associated with epidermal growth factor receptor mutation status in patients with lung adenocarcinoma. *Radiology* 2016;**280**(1):271–80 https://doi:10.1148/radiol.2016151455.
18. Son JY, Lee HY, Kim JH, *et al*. Quantitative CT analysis of pulmonary ground-glass opacity nodules for distinguishing invasive adenocarcinoma from non-invasive or minimally invasive adenocarcinoma: the added value of using iodine mapping. *Eur Radiol* 2016;**26**(1):43–54 https://doi:10.1007/s00330-015-3816-y.
19. Altan M, Chiang AC. Management of small cell lung cancer: progress and updates. *Cancer J* 2015;**21**(5):425–33 https://doi:10.1097/ppo.0000000000000148.
20. Dolly SO, Collins DC, Sundar R, *et al*. Advances in the development of molecularly targeted agents in non-small-cell lung cancer. *Drugs* 2017;**77**(8):813–27 https://doi:10.1007/s40265-017-0732-2.
21. Travis WD. Update on small cell carcinoma and its differentiation from squamous cell carcinoma and other non-small cell carcinomas. *Mod Pathol* 2012;**25**(Suppl. 1):S18–30 https://doi:10.1038/modpathol.2011.150.
22. Kazawa N, Kitaichi M, Hiraoka M, *et al*. Small cell lung carcinoma: eight types of extension and spread on computed tomography. *J Comput Assist Tomogr* 2006;**30**(4):653–61.
23. Lee D, Rho JY, Kang S, *et al*. CT findings of small cell lung carcinoma: can recognizable features be found? *Medicine* 2016;**95**(47):e5426 https://doi:10.1097/md.0000000000005426.
24. Simons D, Kachelriess M, Schlemmer HP. Recent developments of dual-energy CT in oncology. *Eur Radiol* 2014;**24**(4):930–9 https://doi:10.1007/s00330-013-3087-4.
25. Shi J, Schmid-Bindert G, Fink C, *et al*. Dynamic volume perfusion CT in patients with lung cancer: baseline perfusion characteristics of different histological subtypes. *Eur J Radiol* 2013;**82**(12):e894–900 https://doi:10.1016/j.ejrad.2013.08.023.
26. Spira D, Neumeister H, Spira SM, *et al*. Assessment of tumour vascularity in lung cancer using volume perfusion CT (VPCT) with histopathologic comparison: a further step toward an individualized tumour characterization. *J Comput Assist Tomogr* 2013;**37**(1):15–21 https://doi:10.1097/RCT.0b013e318277c84f.
27. Gordic S, Puippe GD, Krauss B, *et al*. Correlation between dual-energy and perfusion CT in patients with hepatocellular carcinoma. *Radiology* 2016;**280**(1):78–87 https://doi:10.1148/radiol.2015151560.
28. Fuld MK, Halaweish AF, Haynes SE, *et al*. Pulmonary perfused blood volume with dual-energy CT as surrogate for pulmonary perfusion assessed with dynamic multidetector CT. *Radiology* 2013;**267**(3):747–56 https://doi:10.1148/radiol.12112789.
29. Lurz M, Lell MM, Wuest W, *et al*. Automated tube voltage selection in thoracoabdominal computed tomography at high pitch using a third-generation dual-source scanner: image quality and radiation dose performance. *Invest Radiol* 2015;**50**(5):352–60 https://doi:10.1097/rli.0000000000000133.
30. Zhu X, Dong D, Chen Z, *et al*. Radiomic signature as a diagnostic factor for histologic subtype classification of non-small cell lung cancer. *Eur Radiol* 2018;**28**(7):2772–8 https://doi:10.1007/s00330-017-5221-1.

31. Huang Y, Liu Z, He L, *et al*. Radiomics signature: a potential biomarker for the prediction of disease-free survival in early-stage (I or II) non-small cell lung cancer. *Radiology* 2016;**281**(3):947–57 https://doi:10.1148/radiol.2016152234.

32. Ma E, Ren A, Gao B, *et al*. ROI for outlining an entire tumour is a reliable approach for quantification of lung cancer tumour vascular parameters using CT perfusion. *OncoTargets Ther* 2016;**9**:2377–92384 https://doi:10.2147/ott.s98060.